INSTITUTE OF PHYSICS PUBLISHING INVERSE PROBLEMS

Inverse Problems **18** (2002) 1–12 PII: S0266-5611(02)34079-6

Equipotential line method for magnetic resonance electrical impedance tomography

Ohin Kwon[1], **June-Yub Lee**[2] **and Jeong-Rock Yoon**[3,4]

[1] Department of Mathematics, Konkuk University, Seoul 143-701, Korea
[2] Department of Mathematics, Ewha Women's University, Seoul 120-750, Korea
[3] School of Mathematics, Korea Institute for Advanced Study, Seoul 130-012, Korea

Received 20 February 2002, in final form 15 May 2002
Published
Online at stacks.iop.org/IP/18/1

Abstract

We consider magnetic resonance electrical impedance tomography, which aims to reconstruct the conductivity distribution using the internal current density furnished by magnetic resonance imaging. We show the uniqueness of the conductivity reconstruction with one measurement imposing the Dirichlet boundary condition. And we propose a fast non-iterative numerical algorithm for the conductivity reconstruction using the internal current vector information. The algorithm is mainly based on efficient numerical construction of equipotential lines. The resulting numerical method is stable in the sense that the error of the computed conductivity is linearly proportional to the input noise level and the introduction of internal current data makes the impedance tomography problem well-posed. We present various numerical examples to show the feasibility of using our method.

(Some figures in this article are in colour only in the electronic version)

1. Introduction

The standard electrical impedance tomography (EIT) problem is that of recovering the interior conductivity distribution σ by means of boundary measurement of the applied current g and the voltage response f. Then the EIT problem is characterized by the following elliptic partial differential equation: See endnote 1

$$\nabla \cdot (\sigma \nabla u) = 0 \qquad \text{in } \Omega, \qquad u = f \text{ on } \partial\Omega \tag{1}$$ See endnote 2

where u is the voltage potential satisfying $\sigma \partial u/\partial \nu|_{\partial\Omega} = g$. Here Ω denotes the cross-section of an electrically conducting body and ν is the outward unit vector normal to $\partial\Omega$. Many theoretical and numerical approaches have been studied during last a couple of decades. Among these we wish to cite [3, 8] and the references therein. However, the EIT problem has not been fully conquered yet due to the fact that it is highly non-linear and severely ill-posed [10, 12].

[4] Current address: Department of Mathematical Sciences, Rensselaer Polytechnic Institute, Troy, NY 12180, USA.

In contrast, a new imaging technique—so-called magnetic resonance electrical impedance tomography (MREIT), suggested by [9]—uses the internal current densities as the data, instead of restricting use to the boundary measurements. These internal current density data are furnished by a recent current density imaging (CDI) technique with the aid of magnetic resonance (MR) imaging. For readers' convenience, we briefly explain the CDI technique. For a more detailed discussion, please refer to [4, 6, 13, 14, 16]. The nuclear spin density $\rho(x, y, z)$ is obtained by the inverse Fourier transformation of the MR signal $S(t_x, t_y, t_z)$ on three-dimensional data acquisition axes (t_x, t_y, t_z):

$$S(t_x, t_y, t_z) = \int_{\mathbb{R}^3} \rho(x, y, z) \exp[-\mathrm{i}\gamma(xG_x t_x + yG_y t_y + zG_z t_z)]\, \mathrm{d}x\, \mathrm{d}y\, \mathrm{d}z$$

where γ is the gyromagnetic ratio and (G_x, G_y, G_z) is the magnetic field gradient. When a current I is injected, a new nuclear spin density ρ_I is given by

$$\rho_I(x, y, z) = \rho(x, y, z) \exp[\mathrm{i}\gamma T_c B_z(x, y, z)]$$

where T_c is the duration of the current pulse and B_z is the z-component of the magnetic field $\boldsymbol{B}$ induced by the input current I. Here the main magnetic field in the MR system is along the z-direction. Comparing the current-injected spin density ρ_I and the no-current-injected spin density ρ, we can calculate B_z from the following phase difference mapping:

$$B_z(x, y, z) = \frac{1}{\gamma T_c} \arctan\left(\frac{\mathrm{Im}(\rho_I/\rho(x, y, z))}{\mathrm{Re}(\rho_I/\rho(x, y, z))}\right).$$

Then the internal current density $\boldsymbol{J}$ is obtained by Ampere's law:

$$\boldsymbol{J} = \frac{1}{\mu}\boldsymbol{\nabla} \times \boldsymbol{B}$$

where μ is the magnetic permeability. If the imaged domain is assumed to be two dimensional, then just using B_z is sufficient for the calculation of $\boldsymbol{J}$, since $\boldsymbol{\nabla} \times \boldsymbol{B} = (\partial_y B_z, -\partial_x B_z, 0)$. However, in general, we need to rotate the imaged object to obtain B_x and B_y as well as B_z for the calculation of $\boldsymbol{J}$. Although there are still some technical difficulties associated with obtaining precise information on $\boldsymbol{J}$ in real experiments, in this paper we begin with the assumption that the current density $\boldsymbol{J}$ can be reliably obtained.

Since MREIT based on the CDI technique utilizes internal data, we may expect the ill-posedness of standard EIT to be significantly reduced in MREIT. Now we define the MREIT problem mathematically. Let Ω be a simply connected bounded Lipschitz domain in $\mathbb{R}^2$. The MREIT problem is recovering the conductivity distribution σ satisfying

$$\boldsymbol{\nabla} \cdot (\sigma \boldsymbol{\nabla} u) = 0 \qquad \text{in } \Omega \tag{1}$$

from the internal current density measurement

$$\boldsymbol{J} = \sigma \boldsymbol{\nabla} u \qquad \text{in } \Omega \tag{2}$$

and some boundary measurements. For convenience, the direction of the current density vector $\boldsymbol{J}$ is defined to be opposite to the physical convention in (2).

The first attempt to reconstruct the conductivity distribution σ using MREIT was made in [9]. Combining (1) and (2), a non-linear partial differential equation was derived:

$$\boldsymbol{\nabla} \cdot \left(\frac{|\boldsymbol{J}|}{|\boldsymbol{\nabla} u|}\boldsymbol{\nabla} u\right) = 0 \qquad \text{in } \Omega \tag{3}$$

and an iterative algorithm developed based on two measurements of the *magnitude* of the interior current density $|\boldsymbol{J}|$. Each iteration accomplished an alternative substitution of the

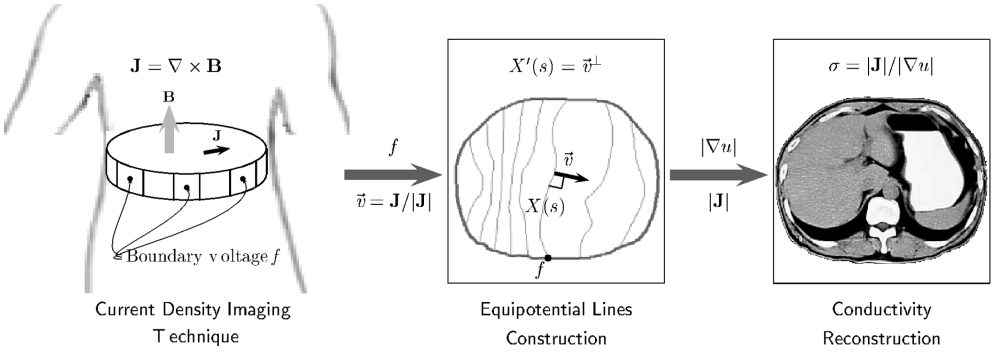

Figure 1. A schematic diagram of the equipotential line method for MREIT.

intermediate conductivity distribution. Because the non-linear partial differential equation (3) has to be solved at each iteration, a fast numerical solver is crucial for this algorithm.

However, our main observation in this paper will be that the efficient numerical algorithm for the MREIT problem has nothing to do with the complicated non-linear partial differential equation (3); meanwhile the core information is readily obtained from (2). Thus our inverse problem will be to reconstruct σ which satisfies

$$\sigma \nabla u = \boldsymbol{J} \qquad \text{in } \Omega, \tag{4}$$

$$u = f \qquad \text{on } \partial\Omega \tag{5}$$

where $(f, \boldsymbol{J})$ are given data. We will propose a non-iterative simple numerical method for recovering σ based on the numerical construction of equipotential lines. While in [7, 9] the authors ignored the *direction* information of the internal current density, we will utilize information on both magnitude and direction.

Now we explain briefly our algorithm, which will be presented in section 3 in detail: with the current density $\boldsymbol{J}$ furnished by the CDI technique, we decompose it into the direction information $\vec{v} = \boldsymbol{J}/|\boldsymbol{J}|$ and the magnitude information $|\boldsymbol{J}|$. Since $\vec{v} = \nabla u/|\nabla u|$ is perpendicular to each equipotential line, we can construct all the equipotential lines $X(s)$ by solving the ordinary differential equation $X'(s) = \vec{v}^{\perp}$ with the boundary condition (5). Here $(\cdot)^{\perp}$ denotes the anticlockwise right-angle rotation. Calculating $|\nabla u|$ using the constructed equipotential lines, we finally reconstruct the conductivity distribution from $\sigma = |\boldsymbol{J}|/|\nabla u|$. A schematic diagram of our method is shown in figure 1.

Before concluding our introduction, we want to comment on the boundary condition: the original MREIT model introduced in [7, 9] was characterized by imposing the Neumann boundary condition $\sigma \partial u/\partial \nu = g$ on $\partial\Omega$. The main reason for imposing the Neumann boundary condition was the experimental ease of measuring the current rather than the voltage measurement. However, it is not difficult to design a *Dirichlet* MREIT model which is characterized by the Dirichlet boundary condition (5). This model is mathematically simpler than the *Neumann* MREIT model and the arguments in this paper also hold for the standard *Neumann* MREIT model if the conductivity on the boundary is also known.

In section 2, we prove the uniqueness of the conductivity in MREIT with one measurement. Recall that in [7, 9] the authors required two measurements to guarantee uniqueness when the Neumann boundary data are specified. In section 3, we describe our equipotential line method and comment on the actual programming. In section 4, we present various numerical examples and discuss the convergence of our method.

2. Uniqueness of Dirichlet-type MREIT

Let $\Omega \subset \mathbb{R}^2$ be a simply connected bounded domain with a $\mathcal{C}^2$ boundary and the conductivity distribution σ satisfying $0 < \sigma(x) < \infty$ for all $x \in \bar{\Omega}$. And we assume the boundary voltage potential $f \in \mathcal{C}(\partial\Omega)$ to satisfy the condition that there exist only one local maximum point and only one local minimum point. That is, there exist two points ξ_0, ξ_1 on $\partial\Omega$ and a portion $\Gamma \subset \partial\Omega$ such that

$$f(\xi_0) = \min_{\partial\Omega} f, \qquad f(\xi_1) = \max_{\partial\Omega} f, \qquad f|_{\Gamma} \text{ and } f|_{\partial\Omega\setminus\Gamma} \text{ are one-to-one functions} \tag{6}$$

which means, roughly speaking, that the boundary voltage potential f is strictly increasing along either route from ξ_0 to ξ_1.

Then by the basic theory of elliptic partial differential equations (see [5, pp 206]), the following classical Dirichlet boundary value problem:

$$\nabla \cdot (\sigma \nabla u) = 0 \qquad \text{in } \Omega, \qquad u = f \text{ on } \partial\Omega \tag{7}$$

has a unique solution u in $\mathcal{C}(\bar{\Omega})$. Moreover, we can show that

$$\nabla u(x) \neq 0 \qquad \text{for all } x \in \Omega$$

under the assumption that the conductivity distribution $\sigma > 0$ belongs to the class

$$\Sigma := \left\{ \sigma = \sigma_0 + \sum_{k=1}^{M} \sigma_k \chi_{D_k} \,\middle|\, \sigma_0 \in \mathcal{C}^{\alpha}(\bar{\Omega}), \sigma_k \in \mathcal{C}^{\alpha}(\bar{D}_k), \sigma_k \neq 0 \text{ on } \partial D_k \right\}$$

where $0 < \alpha < 1$ is a fixed number and χ_{D_k} denotes the characteristic function for inclusions D_k such that $\bar{D}_k \subset \Omega$ has a $\mathcal{C}^2$ boundary and $\bar{D}_k \cap \bar{D}_\ell = \emptyset$ for $k \neq \ell$. Note that this class Σ includes almost all physically meaningful conductivity distributions. In fact, the class Σ was introduced in [7] to show a result analogous to the following lemma for the Neumann boundary value problem, the proof of which can also be found in [1, 2, 15]. Since the proof of the following lemma is parallel to that of Neumann boundary value problem, we only give an outline of it.

Lemma 2.1. *Assume $f \in \mathcal{C}(\partial\Omega)$ satisfying (6) and $\sigma \in \Sigma$. Then the solution u to the classical Dirichlet boundary value problem (7) satisfies*

$$\nabla u(x) \neq 0 \qquad \textit{for all } x \in \Omega.$$

Proof. When $\sigma \in \Sigma$ is expressed by $\sigma = \sigma_0 + \sum_{k=1}^{M} \sigma_k \chi_{D_k}$, then by the standard theory of elliptic equations [5, 11], we know that $\nabla u \in \mathcal{C}^{\alpha}(\cup_{k=1}^{M} \bar{D}_k) \cap \mathcal{C}^{\alpha}(\Omega \setminus \cup_{k=1}^{M} D_k t)$. Thus ∇u is well defined in Ω. Suppose that there exists a point $x_0 \in \Omega$ satisfying $\nabla u(x_0) = 0$. Since the point x_0 is a saddle point of u, the level set $\{x \in \Omega \,|\, u(x) = u(x_0)\}$ divides Ω into at least four disjoint connected components. Applying the maximum principle on each subdivided region, we obtain either a local maximum or local minimum on the intersection of each subregion and the outer boundary $\partial\Omega$. Hence it is a contradiction to (6), since we have admitted only two local extrema. □

The internal current density $\boldsymbol{J} = \sigma \nabla u$ obtained with the aid of the CDI technique is naturally divergence-free and lemma 2.1 shows that $\boldsymbol{J}$ must be nonzero for almost all physically meaningful conductivity distributions ($\sigma \in \Sigma$), if we apply the boundary voltage $f \in \mathcal{C}(\partial\Omega)$ as in (6). With these data $(f, \boldsymbol{J})$, our inverse problem is that of reconstructing $\sigma \in \Sigma$ which satisfies

$$\sigma \nabla u = \boldsymbol{J} \qquad \text{in } \Omega, \qquad u = f \text{ on } \partial\Omega. \tag{8}$$

While the Neumann-type MREIT problem in [7] has examples exhibiting non-uniqueness, our Dirichlet-type MREIT problem (8), utilizing vector information of the interior current density, has a uniqueness result. See endnote 3

Theorem 2.2. *Let $\boldsymbol{J}$ be a nonzero divergence-free vector field in Ω and $f \in \mathcal{C}(\partial\Omega)$. If (σ_1, u_1) and (σ_2, u_2) are two solutions of (8), then we have $u_1 = u_2$ and $\sigma_1 = \sigma_2$.*

Proof. Since $\boldsymbol{J}$ is divergence-free, we can apply the maximum principle for u_1. For any $x \in \Omega$, by the maximum principle and the continuity of u_1, we are able to construct an equipotential curve $X(s)$ satisfying $X(0) = x$, $X(s_f) = x_b$ for some $x_b \in \partial\Omega$, and

$$u_1(X(s)) = u_1(x_b) = f(x_b), \qquad 0 \leqslant s \leqslant s_f.$$

Using the boundary condition $u_1|_{\partial\Omega} = u_2|_{\partial\Omega} = f$ and line integrals of gradient vector fields on the equipotential curve X of u_1, we obtain

$$u_2(x) = u_2(x_b) + \int_X \nabla u_2 \cdot \mathrm{d}\ell = f(x_b) + \int_X \frac{\sigma_1}{\sigma_2} \nabla u_1 \cdot \mathrm{d}\ell = f(x_b) = u_1(x),$$

which implies $u_1 = u_2$. See endnote 4

Since $\boldsymbol{J}$ is nonzero, so are ∇u_1 and ∇u_2. Thus we easily see that

$$0 = \sigma_1 \nabla u_1 - \sigma_2 \nabla u_2 = (\sigma_1 - \sigma_2) \nabla u_1,$$

which yields that $\sigma_1 = \sigma_2$. The proof is complete. □

In the proof of theorem 2.2, a partial differential equation for u_1, such as (7), was used only for the maximum principle, which determined whether we could construct equipotential curves. Hence as long as we may construct the equipotential curves from the data $(f, \boldsymbol{J})$ without trouble, the reconstruction of u or σ has nothing to do with the partial differential equation itself. As seen in the proof of theorem 2.2, the unique reconstruction is based on the construction of the equipotential curve of u; hence one of the efficient algorithms will be constructing the equipotential curves of u using the data $(f, \boldsymbol{J})$. Moreover, it will be a non-iterative scheme and therefore fast and efficient, which is the main goal of this paper.

3. Numerical algorithm

Our algorithm for reconstructing the internal conductivity distribution $\sigma(x)$ consists of following two simple steps which require non-vanishing current density vector field $\boldsymbol{J}|_\Omega$ and boundary measurement of the voltage $f|_{\partial\Omega}$:

(a) Restoration of the potential $u(x_t)$ in $x_t \in \Omega$. Find a boundary point $x_b \in \partial\Omega$ such that $u(x_t) = f(x_b)$ by solving a first-order ordinary differential equation on the equipotential line $X_t(s)$:

$$\frac{\mathrm{d}X_t}{\mathrm{d}s}(s) = \left(\frac{\boldsymbol{J}(X_t(s))}{|\boldsymbol{J}(X_t(s))|} \right)^{\perp} \qquad \text{with } X_t(0) = x_t \text{ and } X_t(s_f) \in \partial\Omega \tag{9}$$

where $(\cdot)^{\perp}$ denotes the anticlockwise right-angle rotation of a vector.

(b) Reconstruction of the conductivity $\sigma(x_t)$ in $x_t \in \Omega$. Calculate $|\nabla u(x_t)|$ using the reconstructed potential values of nearby points; then $\sigma(x_t)$ is the ratio of $|\boldsymbol{J}|$ and $|\nabla u|$:

$$\sigma(x_t) = \frac{|\boldsymbol{J}(x_t)|}{|\nabla u(x_t)|}. \tag{10}$$

We now present a fast numerical scheme using current density data at Cartesian grid points which can be easily tabulated in a conventional MR imaging system. Developing a high-order numerical scheme using data at arbitrary points is nothing more than applying high-order interpolation and numerical differentiation techniques for those points. Our aim in this paper is to present a new idea for reconstructing the internal conductivity profile using MREIT; thus

building a fast, flexible, and accurate computational tool for industrial applications will be the next step of our research.

The computational cost of step (b) is proportional to the number of target points, say N^2 points in two dimension; thus there is not much to be done in terms of computational cost. However, a naive implementation of step (a), such as by applying the Runge–Kutta method to the ordinary differential equations (9) for each target point, would be too expensive, since it takes order-of-N Runge–Kutta steps for each point and order-of-N^3 steps in total. The following recursive algorithm reduces the total computational cost to $\mathrm{O}(N^2)$ by evaluating a potential value using neighbouring potential values which are supposed to be already computed from boundary values.

The formal description of the method is as follows.

Equipotential line method for MREIT

Step 1. *Given data.* Suppose that $J_{ij} = \boldsymbol{J}(x_i, y_j)$ at all interior grid points $(x_i, y_j) \in \Omega$ and the boundary potential data $f_k = f(x_k, y_k)$ at arbitrary boundary points $(x_k, y_k) \in \partial\Omega$ are given.

Step 2. *Restoration of the potential u_{ij}.* Use a second-order Runge–Kutta method with fixed step size, say $h = \frac{1}{4}\Delta x$, to solve the ordinary differential equation

$$X'_{ij}(s) = \vec{v}^{\perp}(X_{ij}(s)), \qquad X_{ij}(0) = (x_i, y_j)$$

until it leaves the bounding box $B_{ij} = [x_{i-1}, x_{i+1}][y_{i-1}, y_{i+1}]$ or the domain Ω. Here $\vec{v}(x, y)$ is a piecewise-bilinear interpolation of v_{mn}:

$$\begin{aligned}\Delta x_m\, \Delta y_n\, \vec{v}(x, y) = {} & (x_{m+1} - x)[(y_{n+1} - y)v_{m,n} + (y - y_n)v_{m,n+1}] \\ & + (x - x_m)[(y_{n+1} - y)v_{m+1,n} + (y - y_n)v_{m+1,n+1}]\end{aligned}$$

where $v_{mn} = J_{mn}/|J_{mn}|$ and $(x, y) \in [x_m, x_{m+1} = x_m + \Delta x_m][y_n, y_{n+1} = y_n + \Delta y_n]$. And set the target potential u_{ij} at the point marked with a square to be the second-order interpolation of potentials at three neighbouring points marked with heavy dots, depending on the exit point in the following three cases.

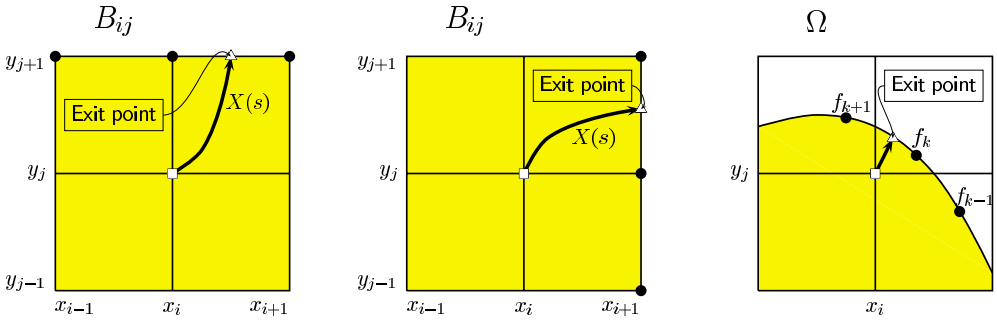

Step 3. *Reconstruction of the conductivity σ_{ij}.* Once potential values at all interior grid points are known, ∇u can be approximated by

$$\nabla u_{ij} = \left(\frac{u_{i+1,j} - u_{i-1,j}}{2\,\Delta x_i}, \ \frac{u_{i,j+1} - u_{i,j-1}}{2\,\Delta y_i} \right).$$

And the conductivity at (x_i, y_j) is just the ratio of $|J_{ij}|$ and $|\nabla u_{ij}|$:

$$\sigma_{ij} = \frac{|J_{ij}|}{|\nabla u_{ij}|}.$$

Many technical issues have to be addressed before discussion of numerical experiments. Bilinear interpolation of $\vec{v}(x, y)$ and second-order numerical differentiation of u_{ij} near the boundary require special care in programming; however, we will not go into detail, since this is trivial. A far more serious issue is that of how to implement step 2. One may apply a fast marching-type algorithm which computes higher potential values first and lower potential values later. A simpler attempt would use a recursive programming method—that is, if any potential for three points near the box exit point is not ready, then evaluate the missing potentials first. However, regardless of the computational order, this algorithm always generates a deadlock between two target points marked with squares in the left-hand-side diagram below if $u_{i-1,j}$ requires $u_{i,j+1}, u_{i,j}, u_{i,j-1}$ and $u_{i,j-1}$ requires $u_{i-1,j}, u_{i,j}, u_{i+1,j}$. In such a case, we switch to linear interpolation using two points (marked with heavy dots) near the box exit point (marked with triangles) shown in right-hand-side figure below. Switching to linear interpolation to avoid the deadlock, our marching always terminates unless the neighbouring current flows in the opposite direction.

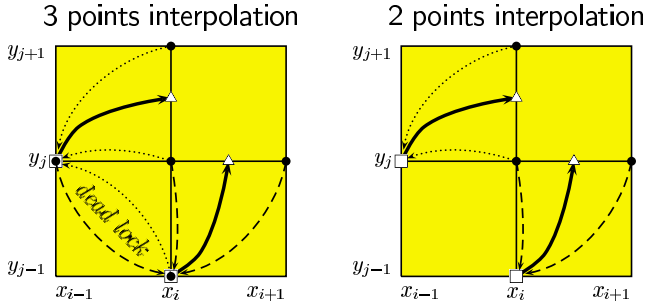

In step 2, the second-order Runge–Kutta method with bilinear interpolation of $\vec{v}(x, y)$ gives a local truncation error of third order and the three-point interpolation method for the potential at the box exit point also gives an error of third order. Thus evaluation of potential values at interior grid points is locally third order in accuracy and globally second order, since the local error can be accumulated at most order-of-N times from the boundary measurements. Because we sometimes use two points instead of three points for the interpolation in order to release the deadlock, the actual order of accuracy for the potential evaluation would be little bit poorer than second order. In step 3, a central difference or three-point one-side numerical differentiation gives second order of accuracy for ∇u if u_{ij} is of locally third order in the absence of input noise in J_{ij}. It is also worth remarking that our algorithm reconstructs the conductivity distribution with errors linearly proportional to the input noise in J_{ij} and f_k for fixed grid size.

4. Numerical examples

The equipotential line method described in the previous section has been implemented in Fortran 77. In this section, we present three numerical examples: the first example shows the numerical accuracy and convergence order of the implementation, the second demonstrates the robustness of the method even for discontinuous conductivity distributions, and the third shows the practical feasibility of using the algorithm for realistic situations. The computational

cost is proportional to the number of grid points, $O(N^2)$, and it takes 0.45–0.58 s to generate figures 2–5, or 6 with 128×128 grid points using an Ultra-60 Sparc station with a 450 MHz CPU.

Example 1 (Smooth conductivity distribution). In this numerical experiment, the conductivity distribution $\sigma \in C^1([-1, 1] \times [-1, 1])$ is given by

$$\sigma(x, y) = 10^{(\sum_{i=1}^{n} w_i \psi_i(x,y))} \tag{11}$$

where the function $\psi_i(x, y)$ supported on $[a_i, b_i][c_i, d_i]$ has the form

$$\psi_i(x, y) = 256 \frac{(x - a_i)^2 (x - b_i)^2}{(a_i - b_i)^4} \frac{(y - c_i)^2 (y - d_i)^2}{(c_i - d_i)^4}.$$

The left figure in figure 2 shows the original conductivity distribution and the right figure visualizes the internal current density data J_{ij} given at 128×128 interior grid points (x_i, y_j) which have been obtained by a standard finite-volume solver for (1) with given injected current source, through the Neumann boundary. Reconstructed potential values and their gradients—using J_{ij} and boundary potential data—are plotted in the middle figure. The contour lines in the right-hand-side figure show the reconstructed conductivity values on a logarithmic scale. Each line represents the same conductivity value of 10 to the power $-1.25, -1.0, \ldots, -0.25$, $0.25, \ldots, 1.25$, respectively. The recovered conductivity has about 2.37% error in a relative l_2-norm.

In the example shown in figure 3, white background noise has been added to the same input data J_{ij} as for figure 2 to check the robustness of our algorithm. 1% additive noise at (x_i, y_j) consists of x-and y-component pairs of random numbers varying from -1 to 1% of $\|J_{ij}\|_{l^2}$. The left figure in figure 3 shows the reconstructed conductivity distribution on a logarithmic scale and the middle and the right plots show the reconstructed conductivity values at $x = 0$ and at $y = 0$ using heavy dots in comparison with the original conductivity shown by solid lines. The method recovers the conductivity distribution successfully with data spoiled by 1% additive noise and the computational result contains 5.87% error in a relative l_2-norm.

Figure 4 shows the convergence of the algorithm in various situations. The first plot demonstrates that the convergence rate is between first order and second order as the number of grid points $2^n \times 2^n$ varies: $n = 5, \ldots, 9$. The middle plot shows the convergence property for the reconstructed conductivity in a noisy environment. It is well known that numerical differentiation with a small grid size may be harmful if there is a high level of errors in the input data, since the total computational error consists of discretization error and noise error which is inversely proportional to the grid size. To overcome the increasing error with a smaller grid size Δx, a higher-order method to compute the gradient ∇u_{ij} should be employed, which gives a relatively small discretization error in ∇u_{ij} even with a relatively large Δx. For fixed grid size Δx, the total error in computing ∇u_{ij} is proportional to the input noise level until it reaches the discretization error. The right figure shows that the method is stable for noise data in the sense that the computational error is proportional to the noise level with fixed grid size $\Delta x = \frac{2}{128}$.

Example 2 (Piecewise-constant conductivity distribution). The circular-shape domain shown in figure 5 contains seven elliptic inclusions of piecewise-constant conductivity. The conductivities of the seven inclusions are 0.1; 5, 30, 5; 20, 0.01, 20 from top to bottom and left to right, respectively, while the background conductivity is 1.

The internal current density J_{ij} and boundary potential f_k were computed with a highly accurate numerical solver using a single-layer integral equation method and then 1% additive white background noise and 10% multiplicative noise were added for the numerical simulation.

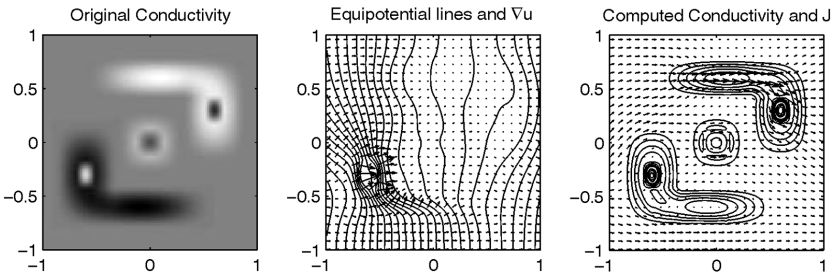

Figure 2. The conductivity distribution for example 1, the computational result for the potential values, and the reconstructed conductivity distribution without noise.

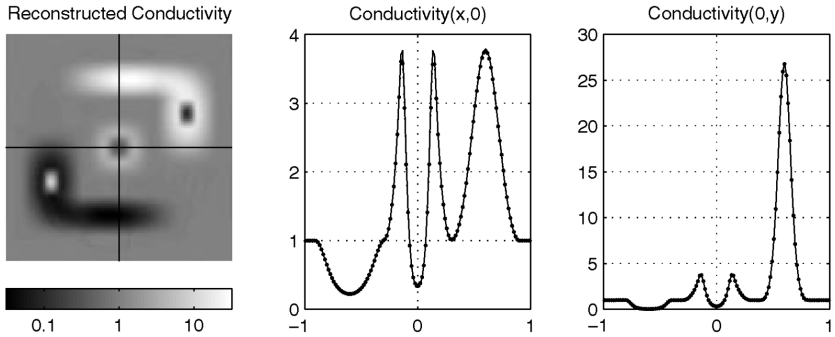

Figure 3. The reconstructed conductivity distribution, using input data J_{ij} with 1% additive noise.

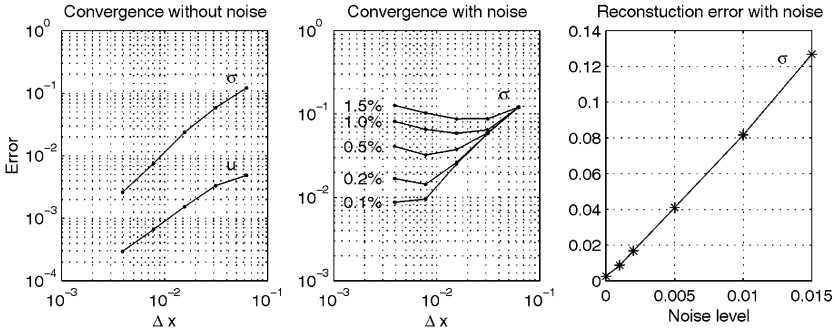

Figure 4. The order of convergence, the convergence result using input data with additive noise, and the numerical stability in a noisy environment.

The 10% multiplicative noise at (x_i, y_j) is a random number pair with the x-and y-components of the random number varying from -10 to $+10\%$ of $|J_{ij}|$.

The upper left figure in figure 5 shows the computed equipotential lines and arrows representing ∇u on the domain with seven elliptic inclusions. The upper right figure shows the reconstructed conductivity on a logarithmic scale. Three lower plots show the cross-sections of the conductivity values at $y = -0.35, 0.0$, and 0.25, respectively. Heavy dots with connecting light dots represent the computed conductivity and solid lines show the original values.

Example 3 (Realistic conductivity distribution). It was not easy to get a real conductivity distribution for a human body, so we assigned conductivity ranging 1–10 to a computerized

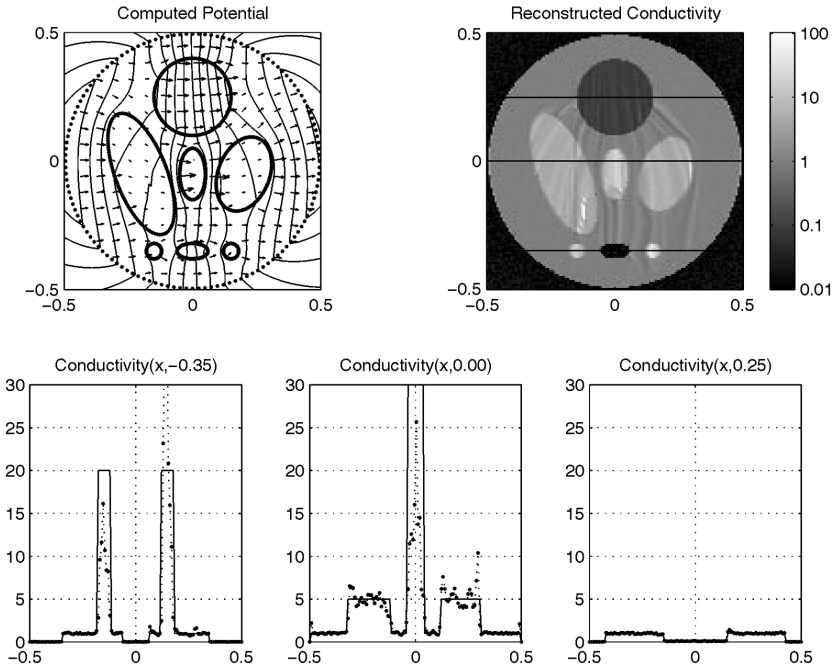

Figure 5. The piecewise-constant conductivity distribution for a phantom with seven inclusions and current density data with 1% additive and 10% multiplicative noise.

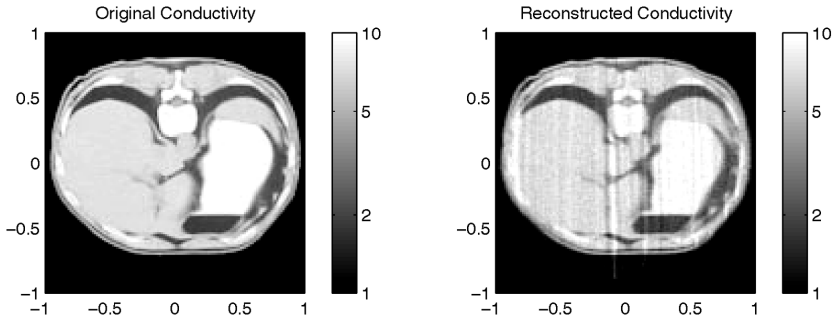

Figure 6. Artificially generated conductivity distributions for the human body with 1% additive and 10% multiplicative noise.

tomography image of a human body with 128×128 pixels shown in figure 6. Current density and boundary data for simulation were obtained using the forward conductivity problem solver used in example 1. It is not related to the conductivity reconstruction problem of a real human body; however, this example simulates the performance of our numerical method in empirical situations.

The left-hand-side figure shows the original conductivity distribution for the simulation. Bright regions represent high conductivity up to 10 and dark regions represent low conductivity down to 1. The right-hand-side figure gives the conductivity distribution reconstructed from a current density data with 1% white background noise and 10% multiplicative measuring error. The relative computational error of the conductivity in an l_2-norm is 12.65%.

5. Conclusions

We implemented a fast, stable, and efficient numerical method for MREIT to reconstruct the conductivity distribution, based on the equipotential line construction. The computational cost is proportional to the number of grid points and the reconstruction error depends linearly on the noise level. As seen in the last graph in figure 4, our problem is no longer ill-posed. It is the usage of the interior data $\boldsymbol{J}$ that enables us to reduce the original ill-posed EIT problem to a well-posed one. The only ill-posed part of our algorithm is computing the gradient of u_{ij}, in which the error due to input noise could be controlled linearly with respect to the noise level using a higher-order numerical differentiation method.

Although the algorithm can also reconstruct discontinuous conductivity distributions, some artefacts such as oscillations or abrupt changes may be found in figure 5. In order to develop a robust method for finding a discontinuous conductivity distribution, we need to pay extra attention to interpolating the directional field $\vec{v}$ and differentiating u near the discontinuity. Also, general interpolation and differentiation tools need to be added to handle the input data at arbitrary points. See endnote 5

A far more serious limitation of our algorithm is that the solver does not work when $|\boldsymbol{J}| = 0$ at any interior point. It is proved in theorem 2.2 that such a situation never arises theoretically with the Dirichlet boundary condition satisfying (6). However, additive noise may render the theorem inapplicable, especially in cases of high conductivity contrast ratio, where the current density $|\boldsymbol{J}|$ in a poorly conducting area would be much smaller than the average current density $\|\boldsymbol{J}\|_{L_2}$. Smoothing the input current density data to arrange for the neighbouring current vectors not to be in opposite directions might be a helpful trick to overcome such a difficulty. Our next step will be developing a robust and high-order solver for application to data for a noisy empirical environment. See endnote 6 See endnote 7

It is worth commenting that the equipotential line method can be naturally extended to three-dimensional problems, although many traditional EIT algorithms become intractable in three-dimensional cases. Equipotential surfaces can be obtained using sequences of equipotential lines from the boundary surface with the current vector field given in the three-dimensional object. Once all equipotential surfaces are known, then the later part of the algorithm is identical to that in the two-dimensional case.

Acknowledgments

The authors thank the anonymous referees very much for their valuable comments which enabled us to improve the quality of this paper. O Kwon was supported by the Faculty Research Fund of Konkuk University in 2001 and J-Y Lee was supported by the Korea Research Foundation under basic science research grant number KRF-2000-015-DP0023.

References

[1] Alessandrini G, Isakov V and Powell J 1995 Local uniqueness in the inverse conductivity problem with one measurement *Trans. Am. Math. Soc.* **347** 3031–41

[2] Alessandrini G and Magnanini R 1992 The index of isolated critical points and solutions of elliptic equations in the plane *Ann. Scuola Norm. Sup. Pisa Cl. Sci.* **19** 567–89

[3] Brühl M and Hanke M 2000 Numerical implementation of two noniterative methods for locating inclusions by impedance tomography *Inverse Problems* **16** 1029–42

[4] Gamba H R and Delpy D T 1998 Measurement of electrical current density distribution within the tissues of the head by magnetic resonance imaging *Med. Biol. Eng. Comput.* **36** 165–70

[5] Gilbarg D and Trudinger N S 1983 *Elliptic Partial Differential Equations of Second Order* (Berlin: Springer)

[6] Ider Y Z and Muftuler L T 1997 Measurement of ac magnetic field distribution using magnetic resonance imaging *IEEE Trans. Med. Imaging* **16** 617–22
[7] Kim S, Kwon O, Seo J K and Yoon J R 2002 On a nonlinear partial differential equation arising in magnetic resonance electrical impedance tomography *SIAM J. Math. Anal.* at press
[8] Kolehmainen V, Voutilainen A and Kaipio J P 2001 Estimation of non-stationary region boundaries in EIT-state estimation approach *Inverse Problems* **17** 1937–56
[9] Kwon O, Woo E, Yoon J R and Seo J K 2002 Magnetic resonance electrical impedance tomography (MREIT): simulation study of J-substitution algorithm *IEEE Trans. Biomed. Eng.* **49** 160–7
[10] Lee J Y and Yoon J R 2001 A numerical method for Cauchy problem using singular value decomposition *Commun. Korean Math. Soc.* **16** 487–508
[11] Ladyzhenskaya O A and Ural'ceva N N 1973 *Linear and Quasilinear Equations of Elliptic Type* (Moscow: Nauka) p 576
[12] Mandache N 2001 Exponential instability in an inverse problem for the Schrödinger equation *Inverse Problems* **17** 1435–44
[13] Scott G C, Joy M L G, Armstrong R L and Henkelman R M 1991 Measurement of nonuniform current density by magnetic resonance *IEEE Trans. Med. Imaging* **10** 362–74
[14] Scott G C, Joy M L G, Armstrong R L and Henkelman R M 1995 Electromagnetic considerations for RF current density imaging *IEEE Trans. Med. Imaging* **14** 515–24
[15] Seo J K 1996 A uniqueness result on inverse conductivity problem with two measurements *J. Fourier Anal. Appl.* **2** 227–35
[16] Woo E J, Lee S Y and Mun C W 1994 Impedance tomography using internal current density distribution measured by nuclear magnetic resonance *Proc. SPIE* **2299** 377–85

See endnote 8

Queries for IOP paper 134079

Journal: **IP**
Author: **O Kwon et al**
Short title: **Equipotential line method for MREIT**

Page 1

Query 1:
Please be aware that the colour figures in this article will only appear in colour in the Web version. If you require colour in the printed journal and have not previously arranged it, please contact the Production Editor now.

Query 2:
Author: 'nabla' made bold (vectorial) throughout—OK?

Page 4

Query 3:
Author: 'uniqueness result' OK? Or change to 'unique result'?

Page 5

Query 4:
Author: Should 'ℓ' (ell) be bold here (2 cases)?

Page 11

Query 5:
Author: Amended wording of these two sentences 'Although the...' OK?

Query 6:
Author: Amended wording 'render the theorem inapplicable' OK?

Query 7:
Author: Any reference yet?

Page 12

Query 8:
Author: Any update for [7]?